

# A large-scale analysis of pockets of open cells and their radiative impact

D. Watson-Parris<sup>1</sup>, S. A. Sutherland<sup>1,2</sup>, M. W. Christensen<sup>1</sup> and P. Stier<sup>1</sup>

<sup>1</sup>Atmospheric, Oceanic and Planetary Physics, Department of Physics, University of Oxford, UK

<sup>2</sup>The University of Sydney, New South Wales, Australia

## Key Points:

- Convolutional Neural Networks are used to detect 8491 pockets of open cells in marine stratocumulus between 2005-2018.
- The first comprehensive analysis of their microphysical and climatological properties is presented.
- Their global radiative effect is found to be negligible. Closing all POCs globally would lead to an instantaneous top-of-atmosphere imbalance of only  $0.02 \text{ W/m}^2$

---

Corresponding author: Duncan Watson-Parris, [duncan.watson-parris@physics.ox.ac.uk](mailto:duncan.watson-parris@physics.ox.ac.uk)

## Abstract

A convolutional neural network was used to detect occurrences of pockets of open cells (POCs). Trained on a small hand-logged dataset and applied to 13 years of satellite imagery the neural network is able to classify 8,491 POCs. This extensive database allows the first robust analysis of the spatial and temporal prevalence of these phenomena, as well as a detailed analysis of their micro-physical properties. We find a large (30%) increase in cloud effective radius inside POCs as compared to their surroundings and similarly large (20%) decrease in cloud fraction. This also allows their global radiative effect to be determined. Using simple radiative approximations we find that the instantaneous global mean top-of-atmosphere perturbation by all POCs is only  $0.02 \text{ W/m}^2$ .

## Plain Language Summary

The amount of sunlight that reaches, and warms, the surface of the earth is heavily influenced by clouds, in particular marine stratocumulus clouds, a type of low-lying cloud that forms above cold-upwelling regions of the ocean. Marine stratocumulus clouds form in two distinct regimes; open-cells and closed-cells. Closed-cell clouds have a higher cloud cover and reflectivity than open-cell clouds. Small pockets of open cell clouds sometimes form within larger regions of closed-cell clouds, these are referred to as 'pockets of open cells'. Here we use machine learning to detect occurrences of this phenomenon and characterise them in a long-term satellite dataset. This allows their effect on the climate to be determined for the first time. Despite substantial local-scale changes in cloud properties we find that their effect on the climate is small.

## 1 Introduction

Stratocumulus clouds play a vital role in the global energy balance (Randall et al., 1984) and can exist in two distinct regimes: open cells and closed cells (Agee et al., 1973), which can be considered two states of a coupled oscillator (Koren & Feingold, 2011). First coined in 2004 (Bretherton et al., 2004), POCs are small regions of open cell clouds embedded in a uniform surrounding deck of closed cell clouds. Despite the importance of the marine stratocumulus decks on the global climate (Randall et al., 1984; Stevens et al., 2005; Hansen et al., 2013), studying POCs poses several difficulties due to their complex and ill defined nature. POCs also cannot be resolved by the general circulation models (GCMs) used to model the global climate due to their relatively small spatial scale (Berner, Bretherton, Wood, & Mulbauer, 2013). The global radiative impact of POCs and hence that of their absence in GCMs is currently unknown.

Closed cells have a markedly higher albedo than open cells due to their increased cloud fraction (Rosenfeld et al., 2006). Factors affecting the open/closed transition could have a dramatic effect on the total contribution of these clouds to the planetary albedo. For example, it has been proposed that anthropogenic aerosol could have a large effect on the number of POCs, and in turn lead to a large top-of-atmosphere radiative perturbation (Rosenfeld et al., 2006).

Since their discovery, many studies have investigated the properties of selected POCs. It has been observed that POCs are coherent and long-lived, lasting tens of hours (Stevens et al., 2005; Berner, Bretherton, Wood, & Mulbauer, 2013; Wang & Feingold, 2009), and typically consisting of fewer, larger cloud droplets than the surrounding cloud (Stevens et al., 2005; Wood et al., 2011; Terai et al., 2014). They locally have a reduction in cloud optical depth, and a stronger tendency to precipitate compared to the surrounding cloud (Stevens et al., 2005; Berner, Bretherton, Wood, & Mulbauer, 2013). The surrounding cloud outside of a POC is moister than in uniform closed cells (Stevens et al., 2005), there is a reduced rate of entrainment drying, and more efficient coalescence scavenging in POCs than in the surrounding cloud (Stevens et al., 2005; Berner, Bretherton, Wood, & Mulbauer,

2013; Wood et al., 2011; Terai et al., 2014). Modelling studies have shown the formation of POCs is likely driven by a sharp increase in collision-coalescence as Liquid Water Path (LWP) increases and cloud droplet number decreases (Berner, Bretherton, Wood, & Muhlbauer, 2013), and is maintained through the enhanced nucleation caused by the very efficient wet removal of aerosol just below the inversion (Kazil et al., 2011).

While painting a consistent picture, each of the observational studies described above include very few POC cases (at most five), and often used data that was not collected specifically for the analysis of POCs. Although one recent analysis presented a large hand-annotated collection of open-cellular cloud cover over the south east Atlantic (Abel et al., 2019), no global analysis of POCs has been performed. Here we use a machine learning technique to automatically detect POCs from satellite images and build up a database of almost 8500 POCs, shedding light for the first time on their spatial and temporal distributions. Using this database we are also able to make robust estimates of the average micro- and macro-physical properties of these phenomena in each of the three main stratocumulus regions of the globe.

We will outline the data used and the machine learning methods applied to the problem in Sec. 2; describe the spatial and temporal distributions of the POCs and their average physical properties in Sec. 3; before concluding in Sec. 4 with a discussion of the implications for these results and an indication of some of the many other possible uses for the database.

## 2 Method

For the POC detection process we use true-color RGB composites generated using SatPy (Raspaud et al., 2018) from the Moderate Resolution Imaging Spectrometer (MODIS) on board the NASA Terra (MODIS Science Team, 2015) satellite. The Level 1B data sets were used which provide calibrated and geolocated radiances for all 36 MODIS spectral bands at 1km resolution. Due to the relatively large size of POCs and to speed up training and detection the images were linearly resampled from 1350x2030 pixels and split in two, producing 224x224 pixel images.

In order to train the machine-learning model it is necessary to create a dataset of satellite images and hand-logged POC masks. However, determining whether a particular pattern in a cloud deck is truly a POC or not can be ambiguous as no clear definition currently exists. In order to ensure that the labelling of the POCs was consistent, a set of rules were devised. These rules were designed to balance the number of falsely identified POCs and the number of missed POCs. The finalised rules are as follows:

1. The structure of the POC and surrounding cloud must be correct: POCs must be open cell cloud, which looks ‘stringy’, and the surrounding cloud must be closed cell cloud, which looks ‘bubbly’. It is often hard to distinguish between a thin layer of closed cell clouds, where the ‘bubbles’ become separated and open cell clouds, but identifying it as one of these two descriptive words helps to decide which it is.
2. At least 80% of the perimeter of the POC must be continuous closed cell cloud. This is still likely a POC, since it has formed mostly embedded, and not requiring a POC to be completely embedded significantly increases the amount of data with which to train the model.
3. POCs can be at the edge of an image. While there is no way of knowing what the cloud deck looks like beyond the bounds of the image, it is beneficial for the neural net to count these as POCs, since they share the same structure and properties as POCs elsewhere, allowing it to learn better.

110 4. The boundary must be ‘reasonably sharp’ on all edges. A sharp transition from  
 111 open to closed cell clouds is characteristic of a POC, and so if this transition was  
 112 too gradual the POC was ignored.

113 Applying these labelling rules to a selection of 1029 images resulted in a dataset  
 114 of 216 images containing 715 POCs, and 813 images that are known to contain no POCs<sup>1</sup>.

115 The model itself uses a modified ResNet-152 (He et al., 2015) with the dense layers  
 116 replaced by three up-sampling blocks based on the second half of the ResUnet model (Zhang  
 117 et al., 2017). The ResNet-152 portion of the model is pre-trained on ImageNet (Deng  
 118 et al., 2009). The upsampling blocks are trained using a DICE loss function and Adam  
 119 optimizer, with a learning rate that decayed by factors of 0.2 when the validation loss  
 120 plateaued for 3 epochs. The final masks are refined using a second, reduced ResUnet,  
 121 model that was trained in the same way as the ResNet-152 model. These models were  
 122 both implemented in Keras (Chollet et al., 2015), using the TensorFlow engine (Abadi  
 123 et al., 2015) and are freely available as described in the Acknowledgements.

124 To gauge the performance of the model in terms of true positives (TP) and neg-  
 125 atives (TN), and false positives (FP) and negatives (FN), a balanced accuracy score is  
 126 used (L. Olson & Delen, 2008):

$$127 \quad \text{bACC} = \frac{1}{2} \left( \frac{\text{TP}}{\text{TP} + \text{FN}} + \frac{\text{TN}}{\text{TN} + \text{FP}} \right). \quad (1)$$

128 These scores were initially calculated on a pixel-by-pixel basis, however the training set  
 129 of POCs was constructed using masks that had straight edges, while the model can track  
 130 the edge of a POC with much greater accuracy. This meant that the model was unfairly  
 131 penalised since the exact shape of the POC did not match up, resulting in greater num-  
 132 bers of false negatives and positives. To combat this, the metrics were calculated using  
 133 whether or not the image contained a POC, since if it did it is likely that the POC was  
 134 placed correctly due to its distinctive nature. The balanced accuracy score of the model  
 135 on the test set of 100 images was 0.863. Therefor any POC identified by the model has  
 136 an 86% chance of being a correct identification, meaning the vast majority of POCs in  
 137 the dataset created by the model are true positives. In other iterations of the model, it  
 138 was possible to get a much higher recall (TP/(TP+FN)), however only to the detriment  
 139 of the precision (TP/(TP+FP)). We choose to prefer ensuring more of the POCs found  
 140 are true positives rather than detecting as many as possible and introducing false pos-  
 141 itives.

142 It should also be noted that, even with the rules enumerated above, labelling POCs  
 143 could often be quite an ambiguous task, and visual inspection confirmed that the net-  
 144 work performed very well. While the masks deviated from the human labels in some places,  
 145 those differences were entirely reasonable and in some cases more accurate than the hu-  
 146 man labelling, as can be seen in Fig. 1.

147 By applying the inferred POC masks to the retrieved MODIS (MOD06\_L2) cloud  
 148 properties (Platnick et al., 2015) we are able to build statistics about the POCs and their  
 149 surrounding environment. Due to their very irregular shapes and sizes it is not possi-  
 150 ble to create an average, or composite POC. Instead, using OpenCV (Bradski, 2000) to  
 151 extract regions of fixed distance from the edge of each POC we can plot the average prop-  
 152 erties as a function of distance from the edges of all of the detected POCs.

---

<sup>1</sup> This resource is being made publicly available - see the Acknowledgments for details.

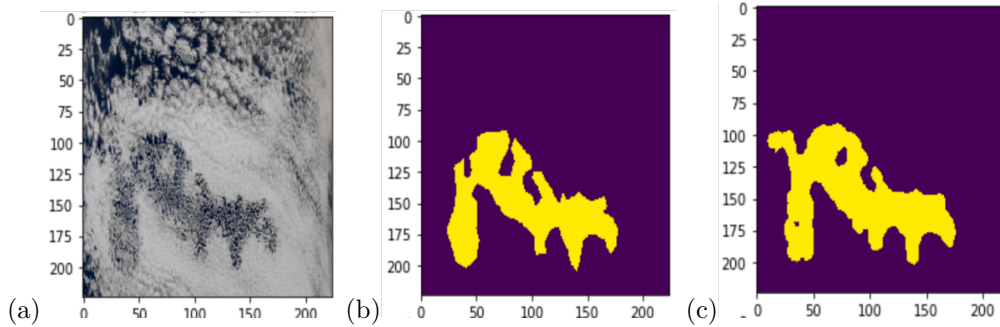


**Figure 1.** From left to right: (a) An example rescaled input image of a POC, (b) the hand logged test mask, and (c) the inferred mask from the machine learning model (which did not see this POC during training).

153

### 3 Results and discussion

154

155

156

157

158

The model was run on all MODIS images which intersected the three main marine stratocumulus regions in the north-east Pacific (off the coast of California), south-east Pacific (off the coast of Peru) and south-east Atlantic (off the coast of Namibia), as defined by Klein and Hartmann (1993), between 2005 to 2018. From the 51,164 images inspected 8,491 POCs were detected, in 4,729 of the images.

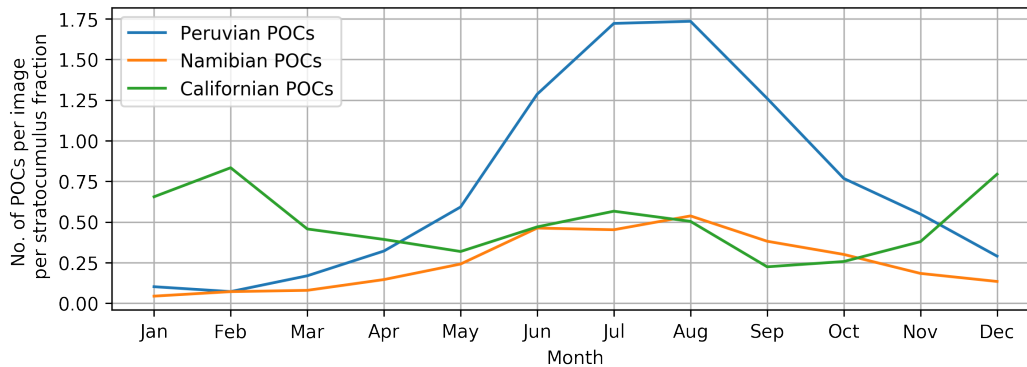


**Figure 2.** Temporal distribution of POC occurrences detected in MODIS true-color imagery by our algorithm for the three regions studied, normalised by the number of images used and the average stratocumulus cloud amount in that region.

159

160

161

162

163

164

165

166

167

Figure 2 shows the temporal distributions of POC occurrence. These have been normalised using the number of images used and the average stratocumulus cloud amount taken from ISCCP data (Young et al., 2018) in order to remove the strong seasonal cycle in the quantity of stratocumulus cloud. One of the most striking features is the magnitude of Peruvian distribution which shows more than three times the number of POCs compared to the other regions. All regions show a well defined peak around local wintertime, coinciding with the maximum stratocumulus amount. The Californian stratocumulus deck, however, also shows a second peak during June to August, the local summertime.

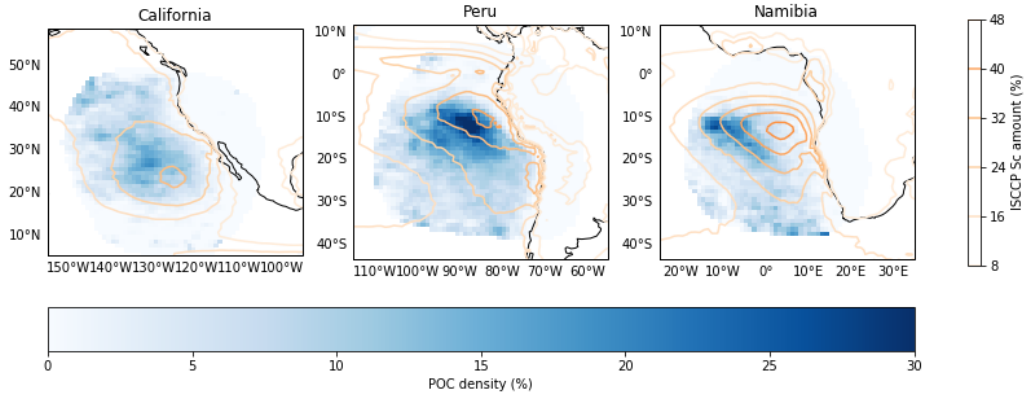


**Figure 3.** The percentage density of detected POCs in the three regions of interest with the ISCCP climatological stratocumulus amount overlaid. Both datasets represent an average between 2005 to 2018.

168 Figure 3 shows the spatial distribution of POCs for the three regions with the average  
 169 ISCCP stratocumulus amount for the same period overlaid. It is interesting to note  
 170 that in the Californian and Namibian cases there appears to be higher densities of POCs  
 171 further from the coast, slightly offset from the peak Sc densities. This could be a consequence  
 172 of the deepening of the boundary layer with increasing sea surface temperature away from coast,  
 173 which favours precipitation and stratocumulus breakup. Off the coast of Namibia, the pattern  
 174 of POC formation is quite distinct, with a clear hotspot that lies away from the centre of the  
 175 climatological stratocumulus distribution. This matches the distribution recently demonstrated  
 176 by Abel et al. (2019), which they attribute to the influence of biomass burning aerosol on the  
 177 open- to closed-cell transition. In the Peruvian case the POC density broadly coincides with  
 178 the main stratocumulus deck.

179 Figure 4 shows the MODIS retrieved mean cloud properties as a function of distance  
 180 from the POC boundary. There are some key features present in these results. Firstly,  
 181 the cloud fraction is lower and varies more within the POC, which is to be expected, since  
 182 cloud fraction is the defining characteristic of a POC. The values obtained here are in  
 183 excellent agreement with detailed in-situ studies Terai et al. (2014) report values of 56-  
 184 83% inside the POC compared to  $\sim 70-80\%$  here. Secondly, the increase in cloud droplet  
 185 effective radius and reduction in cloud optical thickness inside the POCs is also in good  
 186 agreement with previous findings (Stevens et al., 2005). Interestingly, the effective radius  
 187 transitions more slowly than the cloud optical thickness. Since the MODIS retrieved LWP  
 188 is directly proportional to the effective radius multiplied by the optical thickness this leads  
 189 to a dip in the LWP at the edge of the POCs. This could be a tantalising clue as to the  
 190 mechanism for POC formation. However, given the difficulties in retrieving these cloud  
 191 properties in broken cloud scenes and the questionably applicability of adiabaticity  
 192 assumed in the retrievals however, we urge caution in their interpretation. The clear  
 193 decrease in cloud top height within the POCs has not been noted in any previous in-situ  
 194 observations or modelling studies, but may be an artifact due to clear-sky contamination  
 195 in retrieving this property in broken cloud scenes.

196 One property we can be more confident in, and for the first time robustly quantify,  
 197 is the spatial area of the POCs. The probability distributions shown in Fig. 4f show  
 198 a clear multi-modal, log-normal distribution. The peak in the smaller mode occurs at  
 199  $\sim 350\text{km}^2$ , while the larger distribution (containing most of the POCs) peaks at  $\sim 6750\text{km}^2$ .  
 200 It is not clear why POCs should form in these two distinct size regimes.

201 Finally, and perhaps most interestingly, these properties all seem to have no de-  
 202 pendence on region at all, implying that a POC is a universal phenomenon that does not  
 203 depend on its location.

Combining these derived properties with the density distributions, the effect of POC  
 formation on the radiative properties of the stratocumulus decks can be estimated. The  
 albedo of the cloud was calculated using the Eddington approximation (Christensen &  
 Stephens, 2011; Stephens, 1994), and then combined with the cloud fraction to give the  
 overall scene albedo of both the regions inside and outside the POCs:

$$\alpha_c = \frac{(1 - g) \tau_c}{2 + (1 - g) \tau_c}, \quad (2)$$

$$\alpha = f_c \alpha_c + (1 - f_c) \alpha_o, \quad (3)$$

204 where  $\alpha_c$  is the albedo of the cloud,  $\tau_c$  is the cloud optical depth,  $g$  is the asymmetry  
 205 parameter, which for cloud droplets is taken to be  $\sim 0.85$ ,  $\alpha$  is the average albedo for the  
 206 region,  $f_c$  is the cloud fraction, and  $\alpha_o$  is the albedo of the ocean, which was taken to  
 207 be 0.15 in this case. This leads to an albedo of the interior region of POCs ( $\alpha_{\text{POC}}$ ) of  
 208 0.37, whereas the exterior region was calculated to be 0.50 ( $\alpha_{\text{closed cell}}$ ), giving a differ-  
 209 ence of 0.13.

This difference in albedo can be combined with the average incident solar radia-  
 tion ( $R \approx 350 \text{ W m}^{-2}$ ), and the appropriate cloud amounts to estimate the difference in  
 top-of-atmosphere radiation caused by the presence of POCs using:

$$R_{\text{diff}} = R_{\text{inc}} \times (\alpha_{\text{no POCs}} - \alpha_{\text{with POCs}}), \quad (4)$$

$$\alpha_{\text{no POCs}} = |f_{\text{strat}} \alpha_{\text{closed cell}}|, \quad (5)$$

$$\alpha_{\text{with POCs}} = |f_{\text{strat}} (f_{\text{POC}} \alpha_{\text{POC}} + (1 - f_{\text{POC}}) \alpha_{\text{closed cell}})|, \quad (6)$$

210 where  $f_{\text{strat}}$  is the ISCCP stratocumulus amount,  $f_{\text{POC}}$  is the density of POCs and the  
 211 vertical bars represent averages taken over the entire spatial region of available data. This  
 212 leads to an estimate of  $R_{\text{diff}} \approx 0.02 \text{ W m}^{-2}$ . This small value reflects the relatively low  
 213 spatial density of POCs and suggests that any change of POC amount via anthropogenic  
 214 activity (c.f. Rosenfeld et al. (2006)) would not have a large effect on the Earth's radi-  
 215 ation balance. It is possible that the observed POC occurrence is already affected by an-  
 216 thropogenic aerosol, however the similarity in micro-physical properties and rates of oc-  
 217 currence across the different regions would seem to suggest this is unlikely.

## 218 4 Conclusion

219 We have created a global database of all POCs present in three of the main strato-  
 220 cumulus decks over the last 13 years (nearly 8,500) and have analysed their spatial and  
 221 temporal distributions. The properties of the POCs themselves were also studied pro-  
 222 viding significant evidence in support of previous observations of their properties, includ-  
 223 ing a 33% increase in effective radius and a 20% reduction cloud fraction compared to  
 224 the surrounding cloud. The LWP shows a marked reduction at the boundary of the POCs,  
 225 perhaps revealing the effects of precipitation on POC formation, however this retrieval  
 226 is subject to considerable uncertainty in broken scenes. Finally, the properties and cli-  
 227 matology of POCs were combined to obtain an estimated radiative effect of  $0.02 \text{ W m}^{-2}$ ,  
 228 indicating that closing all the POCs in the atmosphere may not have as big an impact  
 229 as previously postulated. These are nevertheless interesting phenomena due to their rel-  
 230 evance for stratocumulus to cumulus transition (with potentially much larger effects) and  
 231 future work tracking POC development and dissipation in geostationary satellite imagery  
 232 should shed light on these mechanisms. The hand-logged training database and auto-  
 233 matically detected POCs are made freely available to the community for further anal-  
 234 ysis.

## Acknowledgments

We gratefully acknowledge the support of Amazon Web Services through an AWS Machine Learning Research Award. We also acknowledge the support of NVIDIA Corporation with the donation of a Titan Xp GPU used for this research. DWP and PS acknowledge funding from the Natural Environment Research Council project NE/L01355X/1 (CLARIFY). PS and MC acknowledge funding from the European Research Council project RECAP under the European Union’s Horizon 2020 research and innovation programme with grant agreement 724602.

The model, including the hand-labeled masks and imagery used for training is available here: <https://github.com/climate-processes/poc-detection>. Our pre-generated POC database is freely available through the JASMIN data portal.

## References

- Abadi, M., Agarwal, A., Barham, P., Brevdo, E., Chen, Z., Citro, C., . . . Zheng, X. (2015). *TensorFlow: Large-scale machine learning on heterogeneous systems*. <https://www.tensorflow.org/>. (Software available from tensorflow.org)
- Abel, S. J., Barrett, P. A., Zuidema, P., Zhang, J., Christensen, M., Peers, F., . . . Flynn, M. (2019). Open cells can decrease the mixing of free-tropospheric biomass burning aerosol into the south-east atlantic boundary layer. *Atmospheric Chemistry and Physics Discussions*, 2019, 1–44. Retrieved from <https://www.atmos-chem-phys-discuss.net/acp-2019-738/> doi: 10.5194/acp-2019-738
- Agee, E. M., Chen, T. S., & Dowell, K. E. (1973). a review of mesoscale cellular convection. *Bulletin of the American Meteorological Society*, 54(10), 1004–1012. Retrieved from [https://doi.org/10.1175/1520-0477\(1973\)054<1004:AROMCC>2.0.CO;2](https://doi.org/10.1175/1520-0477(1973)054<1004:AROMCC>2.0.CO;2) doi: 10.1175/1520-0477(1973)054(1004:AROMCC)2.0.CO;2
- Berner, A. H., Bretherton, C. S., Wood, R., & Muhlbauer, A. (2013). Marine boundary layer cloud regimes and poc formation in a crm coupled to a bulk aerosol scheme. *Atmospheric Chemistry and Physics*, 13(24), 12549–12572. Retrieved from <https://www.atmos-chem-phys.net/13/12549/2013/> doi: 10.5194/acp-13-12549-2013
- Berner, A. H., Bretherton, C. S., Wood, R., & Mulbauer, A. (2013). Marine boundary layer cloud regimes and poc formation in a crm coupled to a bulk aerosol scheme. *Atmospheric Chemistry and Physics*, 13, 12549–12572. Retrieved from <https://doi.org/10.5194/acp-13-12549-2013> doi: 10.5194/acp-13-12549-2013
- Bradski, G. (2000). The OpenCV Library. *Dr. Dobb’s Journal of Software Tools*.
- Bretherton, C. S., Uttal, T., Fairall, C. W., Yuter, S. E., Weller, R. A., Baumgardner, D., . . . Raga, G. B. (2004). The epic 2001 stratocumulus study. *Bulletin of the American Meteorological Society*, 85(7), 967–978. Retrieved from <https://doi.org/10.1175/BAMS-85-7-967> doi: 10.1175/BAMS-85-7-967
- Chollet, F., et al. (2015). *Keras*. <https://keras.io>.
- Christensen, M. W., & Stephens, G. L. (2011). Microphysical and macrophysical responses of marine stratocumulus polluted by underlying ships: Evidence of cloud deepening. *Journal of Geophysical Research: Atmospheres*, 116(D3). Retrieved from <https://agupubs.onlinelibrary.wiley.com/doi/abs/10.1029/2010JD014638> doi: 10.1029/2010JD014638
- Deng, J., Dong, W., Socher, R., Li, L.-J., Li, K., & Fei-Fei, L. (2009). ImageNet: A Large-Scale Hierarchical Image Database. In *Cvpr09*.
- Hansen, J., Laci, A., Rind, D., Russell, G., Stone, P., Fung, I., . . . Lerner, J. (2013). Climate sensitivity: Analysis of feedback mechanisms. In *Climate processes and climate sensitivity* (p. 130–163). American Geophysical Union

- 287 (AGU). Retrieved from <https://agupubs.onlinelibrary.wiley.com/doi/abs/10.1029/GM029p0130> doi: 10.1029/GM029p0130
- 288
- 289 He, K., Zhang, X., Ren, S., & Sun, J. (2015). Deep residual learning for image  
290 recognition. *CoRR*, *abs/1512.03385*. Retrieved from <http://arxiv.org/abs/1512.03385>
- 291
- 292 Kazil, J., Wang, H., Feingold, G., Clarke, A. D., Snider, J. R., & Bandy, A. R.  
293 (2011). Modeling chemical and aerosol processes in the transition from closed  
294 to open cells during vocals-rex. *Atmospheric Chemistry and Physics*, *11*(15),  
295 7491–7514. Retrieved from <https://www.atmos-chem-phys.net/11/7491/2011/> doi: 10.5194/acp-11-7491-2011
- 296
- 297 Klein, S. A., & Hartmann, D. L. (1993). The seasonal cycle of low strat-  
298 iform clouds. *Journal of Climate*, *6*(8), 1587-1606. Retrieved from  
299 [https://doi.org/10.1175/1520-0442\(1993\)006<1587:TSCOLS>2.0.CO;2](https://doi.org/10.1175/1520-0442(1993)006<1587:TSCOLS>2.0.CO;2)  
300 doi: 10.1175/1520-0442(1993)006(1587:TSCOLS)2.0.CO;2
- 301 Koren, I., & Feingold, G. (2011, 7). Aerosolcloudprecipitation system as a predator-  
302 prey problem. *Proceedings of the National Academy of Sciences*, *108*(30),  
303 12227–12232. doi: 10.1073/pnas.1101777108
- 304 L. Olson, D., & Delen, D. (2008). *Advanced data mining techniques* (1st ed.).  
305 Springer-Verlag Berlin Heidelberg. (pp. 138) doi: 10.1007/978-3-540-76917-0
- 306 MODIS Science Team. (2015). *Mod021km modis/terra calibrated radiances 5-min*  
307 *11b swath 1km*. Level 1 and Atmosphere Archive and Distribution System  
308 (LAADS). (<http://modaps.nascom.nasa.gov/services/about/products/c6/MOD021KM.html>) doi: 10.5067/modis/mod021km.006
- 309
- 310 Platnick, S., Ackerman, S. A., King, M. D., Meyer, K., Menzel, W. P., Holz, R. E.,  
311 ... Yang, P. (2015). *Modis atmosphere l2 cloud product (06\_l2)*. NASA  
312 MODIS Adaptive Processing System, Goddard Space Flight Center. Retrieved  
313 from [http://modaps.nascom.nasa.gov/services/about/products/c6/](http://modaps.nascom.nasa.gov/services/about/products/c6/MOD06_L2.html)  
314 [MOD06\\_L2.html](http://modaps.nascom.nasa.gov/services/about/products/c6/MOD06_L2.html) doi: 10.5067/modis/mod06\_l2.006
- 315 Randall, D. A., Coakley, J. A., Fairall, C. W., Kropfli, R. A., & Lenschow, D. H.  
316 (1984). Outlook for research on subtropical marine stratiform clouds. *Bulletin*  
317 *of the American Meteorological Society*, *65*(12), 1290-1301. Retrieved from  
318 [https://doi.org/10.1175/1520-0477\(1984\)065<1290:OFROSM>2.0.CO;2](https://doi.org/10.1175/1520-0477(1984)065<1290:OFROSM>2.0.CO;2)  
319 doi: 10.1175/1520-0477(1984)065(1290:OFROSM)2.0.CO;2
- 320 Raspaud, M., Hoese, D., Dybbroe, A., Lahtinen, P., Devasthale, A., Itkin, M., ...  
321 Thorsteinsson, H. (2018, July). PyTroll: An open-source, community-driven  
322 python framework to process earth observation satellite data. *Bulletin of the*  
323 *American Meteorological Society*, *99*(7), 1329–1336. Retrieved from <https://doi.org/10.1175/bams-d-17-0277.1> doi: 10.1175/bams-d-17-0277.1
- 324
- 325 Rosenfeld, D., Kaufman, Y. J., & Koren, I. (2006). Switching cloud cover and  
326 dynamical regimes from open to closed benard cells in response to the sup-  
327 pression of precipitation by aerosols. *Atmospheric Chemistry and Physics*, *6*,  
328 2503-2511. Retrieved from <https://doi.org/10.5194/acp-6-2503-2006> doi:  
329 10.5194/acp-6-2503-2006
- 330 Stephens, G. (1994). *Remote sensing of the lower atmosphere: An introduction*.  
331 Oxford University Press. Retrieved from [https://books.google.co.uk/books](https://books.google.co.uk/books?id=2FcRAQAIAAJ)  
332 [?id=2FcRAQAIAAJ](https://books.google.co.uk/books?id=2FcRAQAIAAJ)
- 333 Stevens, B., Vali, G., Comstock, K., Wood, R., van Zanten, M. C., Austin, P. H.,  
334 ... Lenschow, D. H. (2005). Pockets of open cells and drizzle in marine  
335 stratocumulus. *Bulletin of the American Meteorological Society*, *86*(1),  
336 51-58. Retrieved from <https://doi.org/10.1175/BAMS-86-1-51> doi:  
337 10.1175/BAMS-86-1-51
- 338 Terai, C. R., Bretherton, C. S., Wood, R., & Painter, G. (2014). Aircraft observa-  
339 tions of aerosol, cloud, precipitation, and boundary layer properties in pockets  
340 of open cells over the southeast pacific. *Atmospheric Chemistry and Physics*,  
341 *14*, 8071-8088. Retrieved from <https://doi.org/10.5194/acp-14-8071-2014>

- 342 doi: 10.5194/acp-14-8071-2014,2014  
343 Wang, H., & Feingold, G. (2009). Modeling mesoscale cellular structures and  
344 drizzle in marine stratocumulus. part i: Impact of drizzle on the formation  
345 and evolution of open cells. *Journal of the Atmospheric Sciences*, *66*(11),  
346 3237-3256. Retrieved from <https://doi.org/10.1175/2009JAS3022.1> doi:  
347 10.1175/2009JAS3022.1
- 348 Wood, R., Bretherton, C. S., Leon, D., Clarke, A. D., Zuidema, P., Allen, G., &  
349 Coe, H. (2011). An aircraft case study of the spatial transition from closed  
350 to open mesoscale cellular convection over the southeast pacific. *Atmospheric*  
351 *Chemistry and Physics*, *11*, 2341-2370. Retrieved from [https://doi.org/](https://doi.org/10.5194/acp-11-2341-2011)  
352 [10.5194/acp-11-2341-2011](https://doi.org/10.5194/acp-11-2341-2011) doi: 10.5194/acp-11-2341-2011
- 353 Young, A. H., Knapp, K. R., Inamdar, A., Hankins, W., & Rossow, W. B. (2018).  
354 The international satellite cloud climatology project h-series climate data  
355 record product. *Earth System Science Data*, *10*(1), 583-593. Retrieved  
356 from <https://www.earth-syst-sci-data.net/10/583/2018/> doi:  
357 10.5194/essd-10-583-2018
- 358 Zhang, Z., Liu, Q., & Wang, Y. (2017). Road extraction by deep residual u-net.  
359 *CoRR*, *abs/1711.10684*. Retrieved from <http://arxiv.org/abs/1711.10684>

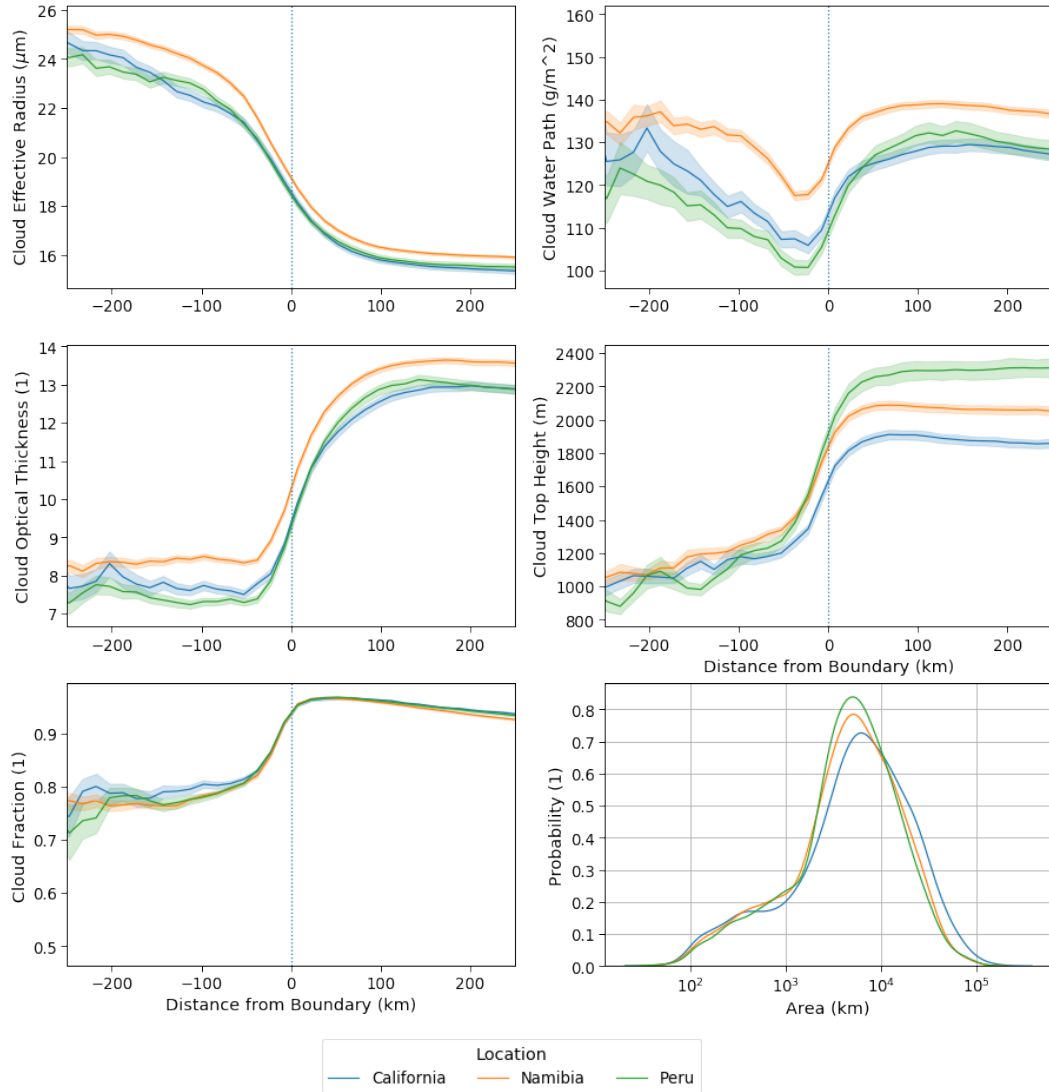


**Figure 4.** MODIS retrieved cloud properties as a function of distance from the boundary of POCs. The vertical line at 0 is the boundary between the POC and the surrounding cloud, with negative values on the x axis being inside the POC and positive values being outside. The different colours represent different geographical regions, and the shaded regions represent the standard error of the data. The final panel shows the probability distribution of the areas of the POCs in each region.

Figure 2.

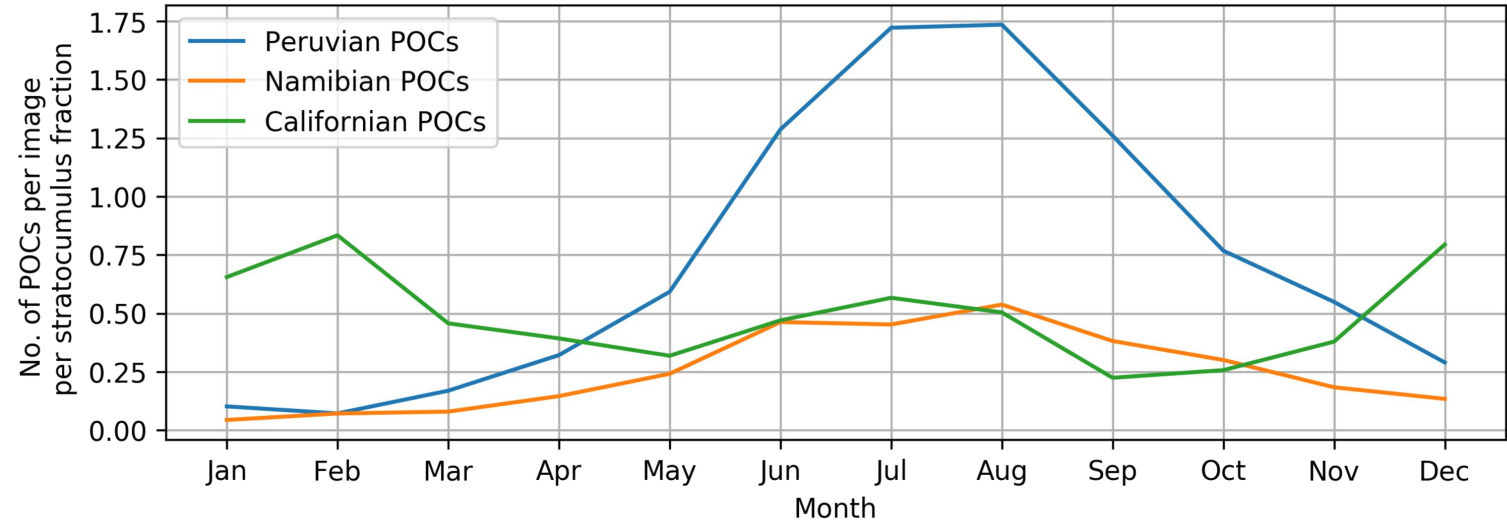


**Figure 1c.**

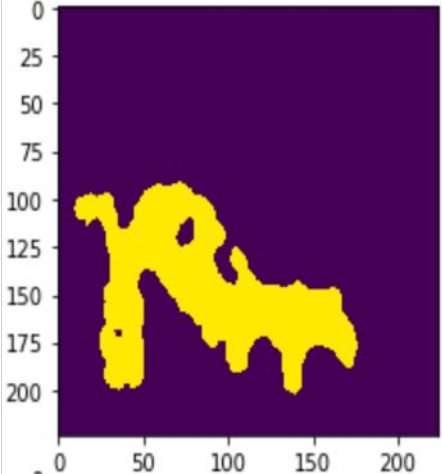


**Figure 4.**

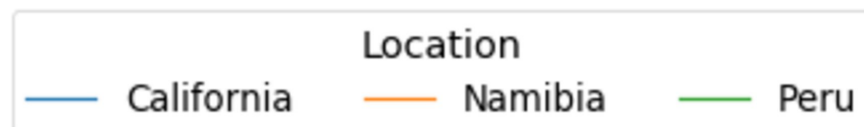
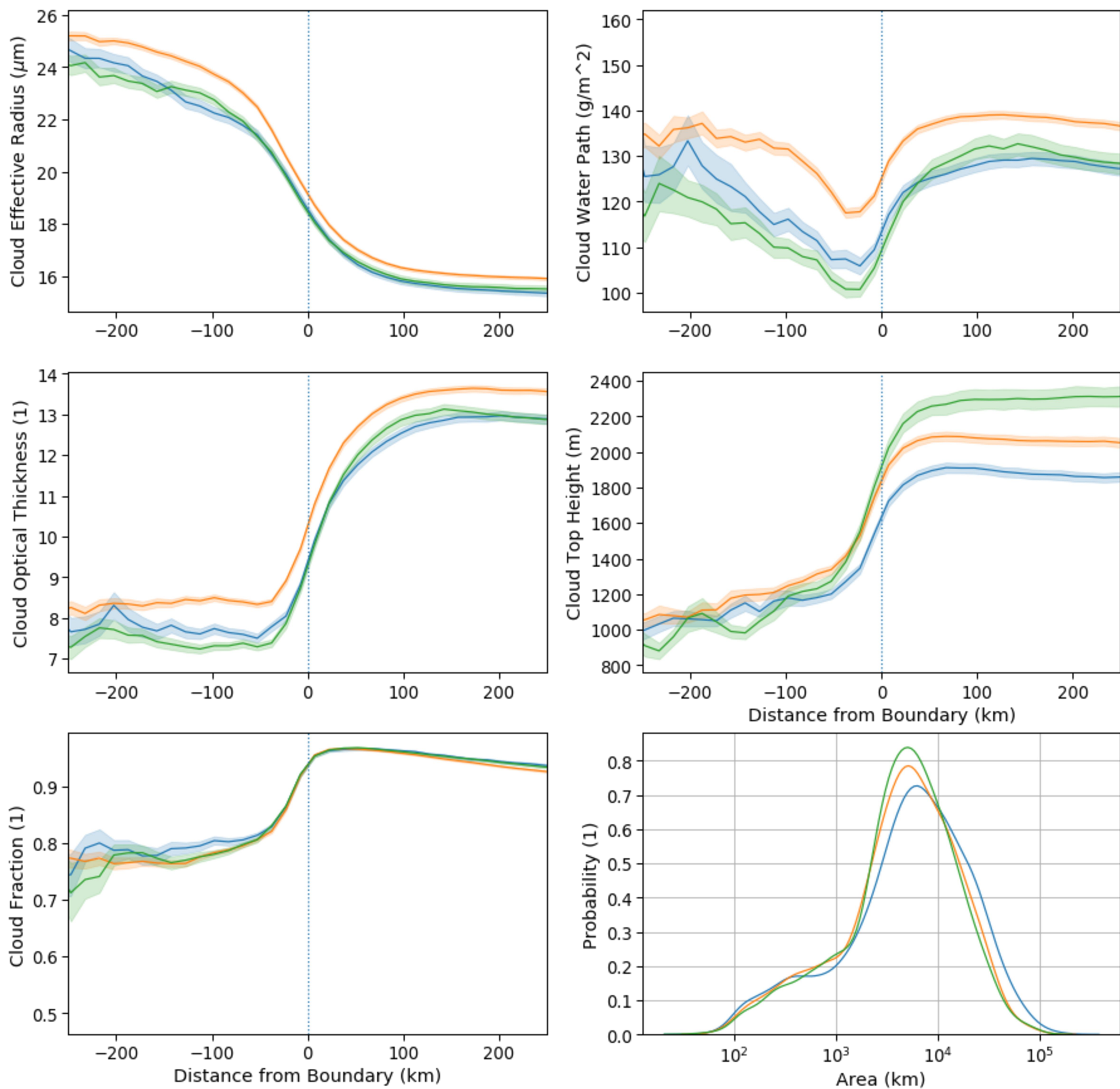
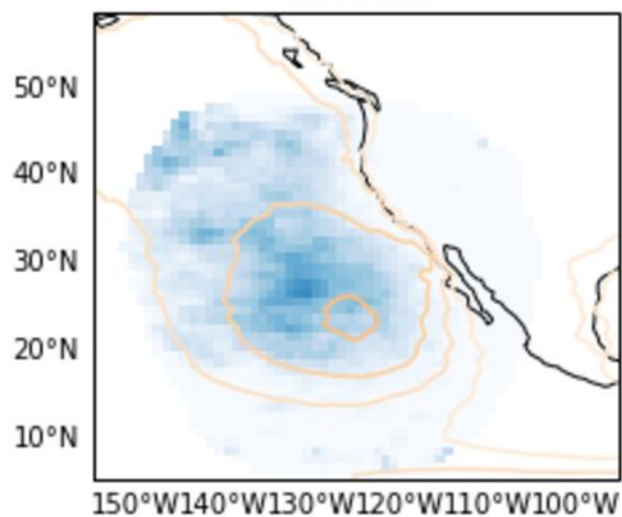
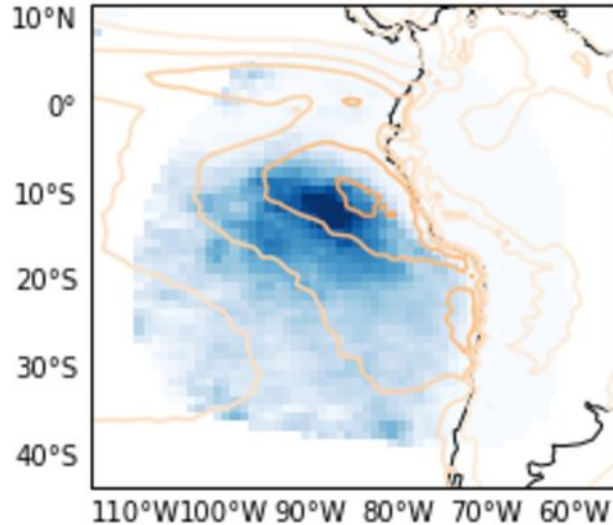


Figure 3.

California



Peru



Namibia

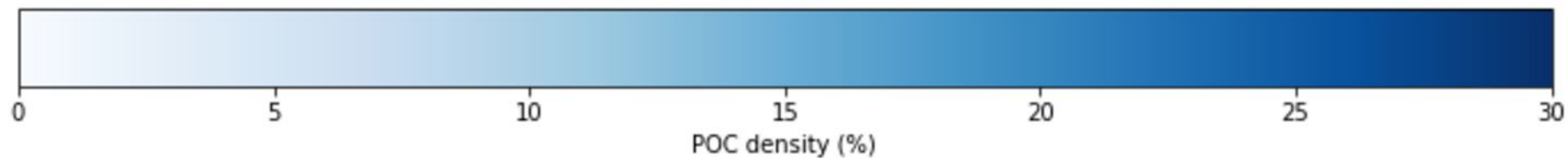
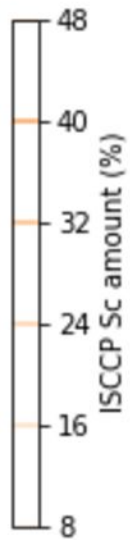
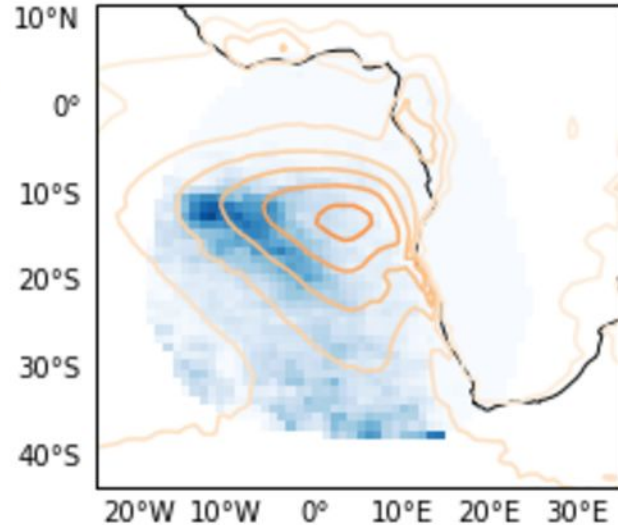


**Figure 1b.**

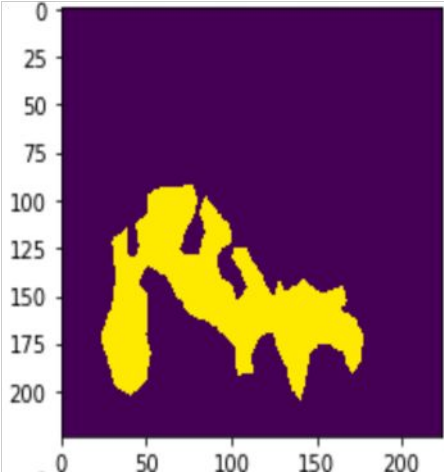


Figure 1a.

